Developmental Biomechanics of Cardiac Looping Morphogenesis

Ashley Miller

May 12, 2025

Abstract

Cardiac looping represents the earliest breaking of left-right symmetry in vertebrates and is a critical milestone in the development of the first functional organ. While its genetic and molecular mechanisms are well-characterized, the biophysical mechanisms have stumped researchers for decades. Here, I compare two mathematical models – one experimental, integrated model and one theoretical, geometric model – for the first phase of cardiac looping in chick embryos.

1 Introduction

Scientists have sought to understand the biophysical mechanisms behind cardiac looping in embryonic development for over a century. As a key milestone in the development of the first functional organ and the earliest visible sign of left-right symmetry breaking, cardiac looping sparks a critical sequence of patterning events essential to healthy embryogenesis. Normal cardiac morphogenesis is contingent on genetic and epigenetic factors, including the surrounding mechanochemical environment [1]. Beyond its importance in understanding organogenesis and symmetry breaking, cardiac looping has undeniable implications for human health as it plays a central role in congenital heart defects, which occur in approximately 1% of live births, 10% of stillbirths, and many first-trimester miscarriages [2]. In addition to the mechanisms driving cardiac looping, researchers are increasingly interested in the functional significance of the heart's complex looped design in both embryonic and mature vertebrates. This architecture may be a solution to packaging constraints, help determine the spatial arrangement of internal organs, or contribute to the optimization of cardiac pumping, which is of particular interest given the early heart tube's valveless pumping function. Some researchers postulate that the kinked looped design provides a pseudo-valve mechanism to promote circulation in the early heart tube. Further, researchers have not definitively proven whether peristalsis – a wave-like muscle contraction – or another mechanism drives pumping in the heart tube [3]. Despite rapid progress in uncovering the molecular and genetic mechanisms behind embryonic heart development, progress in understanding the biomechanical forces and mechanisms that cause cardiac looping remains an open challenge, with numerous hypotheses proposed and discarded over the decades.

2 Morphogenetic Background and Terminology

Cardiac looping is the morphogenetic process by which a straight, pulsating heart tube (HT) transforms into an S-shaped loop during early vertebrate development. The HT arises from the fusion of the left and right heart fields, bilaterally paired regions of the lateral plate mesoderm, along the ventral embryonic midline. By the end of the looping process, the HT has developed an S-shaped, directionally asymmetric configuration. These transformations consist of positional and morphological changes along the dorsoventral, craniocaudal, and left-right (lateral or chiral) axis, followed by final positional adjustments. While cardiac looping and sigmoid routing of the cardiac bloodstream are phylogenetically highly conserved across vertebrates, the final phenotype of the S-shaped loop and the degree of sigmoidal routing can vary considerably across species, as shown in Figure 1. Mature vertebrate hearts can be two-chambered or multichambered. Besides lungfish, all groups of fish have two-chambered hearts with a single atrial and ventricular chamber and a single intra-cardiac flow path. Two-chambered hearts do not regularly show a bilaterally asymmetric/chiral anatomy, which may be due to a packing constraint. Meanwhile, multichambered hearts can be either three-chambered (single ventricle and two atria) or four-chambered (two atria and two ventricles) [3].

Cardiac looping was first observed and studied in chick embryos due to their accessibility for observation. However, researchers have used various model organisms, including fish, amphibians, birds, mammals, and reptiles [3]. Beyond the accessibility of the embryo for observation and manipulation, chick embryonic cardiac looping has been a preferred model organism as it closely parallels human cardiac looping, offers precise staging, and has a well-characterized morphogenesis. Further, the chick embryo can be cultured both in vivo and in vitro to observe cardiac development [4]. This review focuses on modeling efforts in the chick and thus introduces key morphological features and terminology related to the chick heart development.

Using the Hamburger and Hamilton system, which divides the 21-day incubation period of chicks into 46 stages, Figure 2 shows images of the chick embryo HT transformations from stage 10 to 16. At stage 5 (approximately 20 hours), precardiac mesodermal cells migrate anteriorly and medially to form epithelial sheets, which fold into the early HT. By

stages 7-10 (24-36 hours), the HT and primitive foregut develop via bilateral folding and merging, followed by secretion of an extracellular matrix (ECM) known as the cardiac jelly (CJ). Initially, HT consists of three layers: an inner layer of endocardium (EN), a middle layer of CJ, and an outer layer of myocardium (MY). Cardiac looping begins at stage 10 and consists of two phases: C-looping (stages 9-13, 30-50 hours) and S-looping (stages 14-18, 52-68 hours). Blood flow begins by stage 12 (1.9 days). During C-looping, the HT transforms into a C-shaped tube via two main deformations: ventral bending and dextral/rightward torsion, and the original ventral surface of the HT becomes the outer curvature of the looped heart. In contrast, the original dorsal side becomes the inner curvature. In S-looping, the atrium moves superior to the ventricle, establishing the basic form for the mature heart, which forms in stages 21-36 (3.5-10 days) when septation divides the tube into four chambers. Externally, the heart is constrained by several anatomical features, including the omphalomesenteric veins (OVs) at the caudal and cranial end and the dorsal mesocardium (D) – a longitudinal structure attaching the entire length of the heart to the embryo and endodermal layer [1].

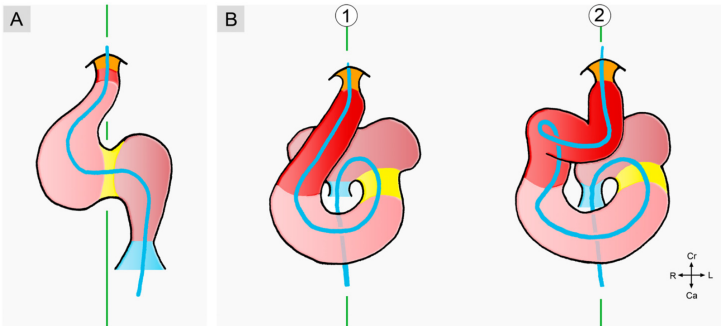

Figure 1: Three basic types of S-loops found in vertebrates. The blue line depicts cardiac flow path, the green line marks the body midline, blue regions are the confluence of veins, brown regions are the atrial segments, yellow regions are the atrioventricular canals, pink regions are the ventricular segments, red regions are ventricular outflow elements, and the orange color marks the distal/non-myocardial portion of the embryonic outflow tract. (A) shows the planar S-loop found in cyclostomes and modern ray-finned fishes, while (B1) shows the simple helical S-loop found in cartilaginous fish and primitive ray-finned fishes, and (B2) shows the complex helical S-loops found in lungfishes and tetrapods [3].

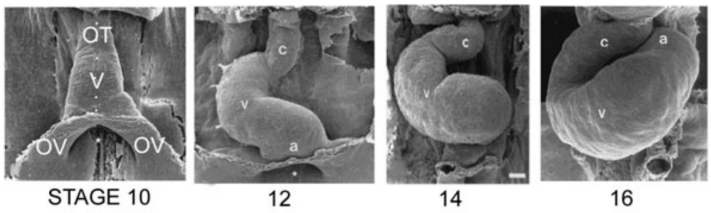

Figure 2: Ventral views of cardiac looping in the chick embryo at stages 10, 12, 14, and 16, where a is atrium, c is conotruncus, OT is outflow tract, OV is omphalomesenteric veins, and V is ventricle [1].

3 Foundational Theories and Experimental Observations

Early efforts to explain cardiac looping focused primarily on descriptive morphology to understand the biophysical drivers of cardiac morphogenesis. At the same time, recent decades have shown increasing interest and progress in identifying the molecular and genetic aspects of cardiac morphogenesis. More recently, researchers have hoped to overcome the stalled progress in uncovering the developmental biomechanics of cardiac morphogenesis using computational and numerical approaches to model key milestones like cardiac looping in well-characterized model vertebrate organisms. Beyond describing the physical mechanisms and forces driving cardiac looping, researchers hope to pinpoint the biological and functional significance of the looped cardiac design.

From a functional standpoint, cardiac looping has typically been viewed as a key driver of left-right symmetry breaking and establishment of pulmonary and circulatory anatomy in the mature organism. Specifically, in the multichambered heart, researchers found that chiral looping influences atrioventricular and ventriculoarterial connections, and abnormalities in looping can cause congenital defects in cardiac flow paths. Researchers have also postulated that looping increases

cardiac pumping efficiency via more favorable outflow tract geometry, optimized venous return positioning with gravity, and minimizes inflow momentum loss. Nonetheless, computational models have failed to confirm any of these theories so far, and researchers are calling for more definitive comparative studies and simulations between looped and unlooped geometries [3].

Using the chick embryo, researchers have done numerous experimental studies involving perturbations to normal cardiac looping to use the process of elimination to confirm or deny various mechanisms for cardiac looping in vertebrates. In normal development, looping begins at the onset of myofibrillogenesis. C-looping consists of ventral bending and rightward/dextral torsion of the HT. Using histological and molecular studies, researchers found thickening of the MY at the inner curvature and thinning at the outer curvature related to actin and cytoskeletal elements. Specific actin arrangements (e.g., circumferential bundles on the inner curvature) arise before and during looping. There are no clear patterns of differential cell division or death in the looping heart. Throughout experiments perturbing aspects of the looping process, researchers have begun identifying intrinsic and extrinsic looping mechanisms. Isolated HTs still bend but do not twist, indicating that bending is intrinsic but torsion is extrinsic. Additionally, splanchopleure (SPL) disruption affects looping direction only when performed on the right side, indicating that mechanical asymmetry is an important constraint. Historical theories include differential growth, hemodynamic forces, cytoskeletal contraction, and cell shape changes as mechanisms for C-looping. Differential growth models suggested uneven cell proliferation at the outer curvature, but studies showed no consistent pattern or regional differences in cell division and death. Researchers postulated that cell shape changes observed (flattening at the outer curvature and radial elongation at the inner side) could be behind looping, but this has yet to be proven experimentally. Other researchers postulated that hemodynamic forces cause looping, which was disproven when they observed looping in embryos with an arrested heartbeat and no circulation. Finally, cytoskeletal contraction was considered critical in looping, but inhibiting actomyosin activity did not prevent bending [1].

Further, while myocardial contraction and cytoskeletal tension are not strictly required for looping, actin polymerization has become a likely driver of ventral bending. Further, studies showed that SPL and OVs influence torsion during early C-looping because, when the SPL is removed, the heart immediately springs back toward the midline and slowly untwists, and, if the OVs are severed, the remainder of the twist disappears, suggesting that the OVs force the HT slightly rightward. At the same time, the SPL pushes it dorsally and further rightward as it rotates about the DM. Based on these conclusions, in 2006, Taber and colleagues proposed an integrated, three-part hypothesis for C-looping. First, at approximately stage 10, cytoskeletal contraction in the caudal OVs generates mechanical stresses which pull the precardiac mesoderm toward the heart, guiding cell migration along fibronectin-aligned stress lines. Next, incoming cells from the OVs asymmetrically push against the caudal HT, forming the future left ventricle and atrium, causing a constrained rightward rotation of the heart by the DM. Finally, ventral bending of the HT is driven by actin polymerization while the SPL appies compressive forces, eventualy rupturing the DM and enabling the full C-shaped configuration. Further, Taber and colleagues suspected that there were redundant asymmetries in the design of the looped HT [1].

4 Mathematical Modeling Approaches

4.1 Integrated Multiphysics Finite-Element Model

Building upon the mechanical hypothesis proposed by Taber in 2006, Shi et al. (2014) developed a comprehensive hypothesis for the biophysical mechanisms of C-looping, which they tested with a finite element model informed by empirical experimental observations. They constructed their model using realistic 3D geometry of the embryonic chick heart, reconstructed from optical coherence tomography (OCT) images at Hamburger-Hilton stage 10. As shown in Figure 3, the authors meshed different regions of the HT, applying specific constraints and morphological processes to each. To describe the complex and, still, unexplained biophysical underpinnings of the bending and torsion in C-looping, they incorporated differential hypertrophic growth in the MY, cytoskeletal contraction in the OVs, and compressive loads from the SPL, populating the model of each process using empirical data gathered by experiments over the decades. This model offered a valuable advance by integrating realistic geometry with the foundational principles of soft tissue biomechanics – specifically, large deformations, growth, and active contraction. Earlier studies by the Taber lab and others suggested that the HT's ventral bending is mainly driven by differential myocardial growth and, less significantly, CJ swelling, myocardial cell shape changes, and DM tension. Meanwhile, researchers widely speculated that the torsional component of C-looping originates from redundant mechanisms, including torque generated by asymmetric OV growth (particularly the relative enlargement of the left OV), cytoskeletal contraction, and external compression from the SPL [2]. Shi et al.'s model allowed for novel, validated experiments on the effects of perturbations on C-looping.

Mathematically, Shi et al.'s 2014 model draws from the theory of morphoelasticity, which separates the total deformation into growth-induced and elastic components. The total deformation gradient, $\mathbf{F}$, represents the mapping from the reference, baseline stage 10 configuration to the final, current, deformed configuration (including all morphological processes applied to the HT). Typically, the deformation gradient tensor is decomposed into 'intermediate' stages in terms of the morphogenesis tensor describing unconstrained, stress-free growth and the elastic deformation gradient tensor, which represents the necessary deformations that would need to be applied to the stress-free configuration to achieve geometric compatibility. Here, Shi et al. refer to the morphogenesis tensor as $\mathbf{M} = (\mathbf{F}^*)^{-1} \cdot \mathbf{F}$, where $\mathbf{F}^*$ is the elastic deformation tensor. Thus, the decomposition of the total deformation gradient tensor would be $\mathbf{F} = \mathbf{F}^*\mathbf{M}$. This morphoelasticity mathematical technique can be visualized as splitting the morphological processes into smaller steps: growth causes a stress-free expansion, elastic recoil brings the tissue back into force balance with surrounding constraints, and perturbations to the looping process cause additional deformations. In fact, Shi et al. use separate morphogenesis tensors to represent the processes which, according to their theories, produce the baseline stage 10 configuration, including endodermal contraction, CJ growth, DM tension, myocardial differential growth, myocardial cell-shape change, OV fusion, and growth in the OVs and CT, which they apply to specific regions meshed and delineated in their 3D model. The Cauchy stress tensor is assumed to depend on only $\mathbf{F}^*$ (as is customary in morphoelasticity) through the constitutive relation,

$$\boldsymbol{\sigma} = \frac{1}{J^*}\,\mathbf{F}^* \cdot \frac{\partial W}{\partial \mathbf{E}^*} \cdot \mathbf{F}^{*T} \tag{1}$$

Here, $J^* = \det(\mathbf{F}^*)$ is the elastic volume ratio, and $\mathbf{E}^* = \frac{1}{2}\left(\mathbf{F}^{*T} \cdot \mathbf{F}^* - \mathbf{I}\right)$ is the elastic Green-Lagrange strain tensor. The material is assumed to be pseudoelastic and isotropic. The strain energy density function W is based on microindentation measurements from chick MY and CJ, and is given by the compressible exponential form:

$$W = \frac{A}{B}\left(e^{B(\bar{I}_1 - 3)} - 1\right) + \frac{1}{D}\left(\frac{J^{*2} - 1}{2} - \ln J^*\right), \tag{2}$$

where A and B are material constants determining the stiffness, D is a bulk modulus-related constant that penalizes volume change, and $J^* = \det(\mathbf{F}^*)$ as before. The term $\bar{I}_1$ is the first modified invariant of the elastic right Cauchy-Green deformation tensor, adjusted for incompressibility, and is defined as: $\bar{I}_1 = J^{*-2/3}\,\mathrm{tr}(\mathbf{F}^{*T} \cdot \mathbf{F}^*)$. This form of W ensures that the material exhibits nonlinear stiffening under large strains while allowing for some compressibility. The authors defined the material properties using indentation experiment data and by considering the types of loads present in different regions. The authors chose boundary conditions to reflect anatomical constraints; for example, the DM was anchored at its ends but allowed to deform elsewhere, the SPL was in frictionless contact with the HT, etc. Using this baseline setup, they validated their model against experimental results by comparing rotation, time history of regional longitudinal strain, and time history of regional circumferential strain between the two, demonstrating close, qualitative agreement. Further, the authors tested the effects of inhibiting contraction and vein fusion. In the experiment, inhibiting non-muscle myosin contraction inhibits looping when applied before stage 10, but does not change looping after stage 10. In the simulation, their initial results did not match these experimental results when turning off contraction or OV fusion. Thus, the authors added cranial-caudal rollers along the boundaries of the DM to produce buckling seen in experiment [2].

After validating their baseline model, Shi et al. experimented with various perturbations of the HT to visualize their effects on C-looping and compare with experimental results of previous works. First, in agreement with experimental results, simulated SPL removal reduced torsion, but did not entirely remove it, indicating that SPL pressure contributes to, but is not totally responsible for, torsion. Next, the researchers tested OV asymmetry by removing the left OV, which reversed the torsion direction (twisting left instead of right), displaying the importance of left-right asymmetry in the OVs for proper C-looping. This result matched the experimental results, besides minor differences in the remaining vein structure. When Shi et al. removed the DM to simulate a lack of DM tension, there was less pronounced bending, indicating it has a minor, additive role in stabilizing the final loop shape. Previous researchers have proposed that observed HT rotation in the absence of the SPL and both OVs happens due to a contractile response on the right side of the HT when the SPL is removed. While the simulated model did not include a contractile force, it did show that the initial left-right asymmetry, combined with the modeled constraints, can contribute to this torsion. Finally, the authors tested the effects of removing the OVs or HT in simulation and compared the results to previous experimental observations. While the simulated model did not include the downstream result of vein fusion seen in the experiment, it did qualitatively reproduce the morphology after left OV removal, right OV removal, both OV removal, and HT removal very well [2].

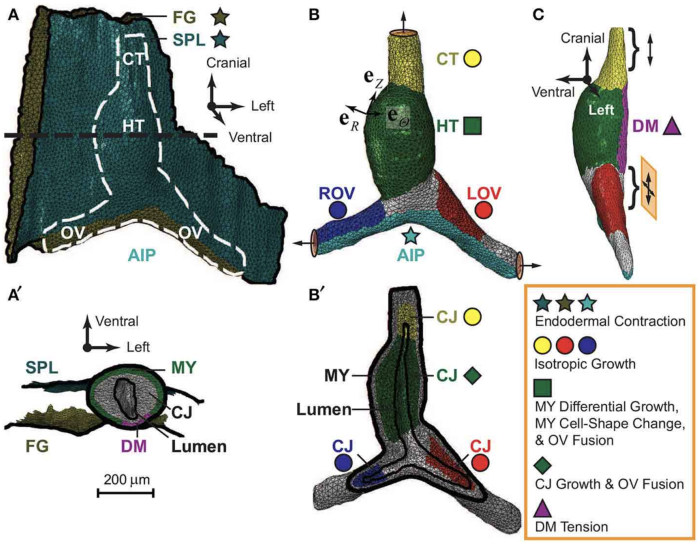

Figure 3: Finite element model of the stage 10 embryonic chick heart reconstructed from OCT images. The heart tube is modeled with surrounding membranes—the splanchnopleure (SPL) and foregut wall (FG)—and includes key anatomical regions: the heart tube (HT), conotruncus (CT), and left/right omphalomesenteric veins (LOV, ROV). Boundary conditions include attachments at the anterior intestinal portal and sliding or constrained motion at specific ends. Morphogenetic processes are applied regionally within the myocardium (MY) and cardiac jelly (CJ), with frictionless contact enforced at membrane interfaces [2].

4.2 Remodeling-Induced Buckling Instability Model

Despite the progress made in Shi et al.'s 2014 model and by other researchers, the biophysical mechanisms behind cardiac looping have remained elusive throughout the past decade. Recently, in 2021, Bevilacqua et al. used linear stability analysis of the nonlinear elastic boundary value problem to determine the onset of C-looping as a function of the geometrical parameters of the fully nonlinear morphological transition, followed by numerical simulations of postbuckling behavior. This original modeling paper focused on simulating the torsional aspects of C-looping, hypothesizing that the spontaneous morphological transition could be modeled as a mechanical instability due to an accumulation of residual stresses arising from the geometrical frustration imposed by tissue remodeling. When developing their model, Bevilacqua et al. assumed the HT is a nonlinear, elastic, homogeneous, incompressible body subjected to finite torsional remodeling, which mimics the cell flux in the HT [4].

The remodeling-induced buckling instability model and experiments consist of a nonlinear elastic model of the HT, a linear stability analysis of the radially symmetric solution, and an implementation of the model in finite element numerical simulations. Bevilacqua et al. modeled the HT geometrically as a homogeneous, one-layered, hollow cylinder with internal radius R_i, external radius R_o, and height L. The reference configuration of the tube is defined in cylindrical coordinates (with $\mathbf{X}$ as the material position coordinate) as $\Omega_0 = \{X = [R\cos\Theta, R\sin\Theta, Z] \in \mathbb{R}^3 \mid R_i \leq R < R_o,\ 0 \leq \Theta < 2\pi,\ 0 < Z < L\}$. The deformation field is indicated by φ such that the actual configuration of the body Ω is given by $\varphi(\Omega)$ and the actual position is given by $\mathbf{x} = \varphi(\mathbf{X})$. Similar to the morphoelasticity theory used in the Shi et al. (2014) paper, to describe the tissue remodeling that induces torsion, the authors define the deformation gradient $\mathbf{F}$ as the decomposition, $\mathbf{F} = \mathbf{F}_e\mathbf{G}$, where $\mathbf{G}$ is the remodeling distortion tensor and $\mathbf{F}_e$ represents the elastic response (often denoted as F^*). The remodeling is defined by

$$\mathbf{G} = \begin{bmatrix} 1 & 0 & 0 \\ 0 & 1 & -\gamma R \\ 0 & 0 & 1 \end{bmatrix}, \tag{3}$$

where γ is the finite torsion rate induced by the remodeling process. Here, G is similar to the "morphogenesis tensor" to describe the torsion process during C-looping. The model enforces incompressibility through the constraint,

$$det\mathbf{F}_e = 1, \tag{4}$$

(sometimes referred to as J). Finally, the authors assume the cylinder cannot elongate along the z-direction, thus $z(Z =$

$0) = 0, \quad z(Z = L) = L$ [4].

Next, to set up the boundary value problem (BVP), the HT is modeled as an isotropic, homogeneous, hyperelastic material with strain energy density W. Specifically, they modeled the material as neo-Hookean with strain energy density $W(\mathbf{F}) = \frac{\mu}{2}\det(\mathbf{G})\left[\text{tr}(\mathbf{F}_e^\top \mathbf{F}_e) - 3\right]$, where μ is the shear modulus. Accordingly, the first Piola–Kirchhoff stress tensor is $\mathbf{P} = \mu \det(\mathbf{G})\,\mathbf{G}^{-1}\mathbf{G}^{-T}\mathbf{F}^\top - p\mathbf{F}^{-1}$, where p is the Lagrange multiplier, which is the necessary hydrostatic pressure to enforce incompressibility. Additionally, the Cauchy stress tensor (comparable with σ from the previous model) is $\mathbf{T} = \mu\mathbf{F}\mathbf{G}^{-1}\mathbf{G}^{-T}\mathbf{F}^\top - p\mathbf{I}$. In the absence of external forces and at quasi-static conditions, the balance of linear momentum results in the following nonlinear system of equations,

$$\text{Div}\,\mathbf{P} = 0 \quad \text{in } \Omega_0, \quad \text{or equivalently} \quad \text{div}\,\mathbf{T} = 0 \quad \text{in } \Omega, \tag{5}$$

where Div is the divergence operator in the material frame, and div is the same operator in the current frame. Further, the authors apply a Neumann (traction-free) condition on the inner and outer boundaries, which, in the Lagrangian frame, is

$$\mathbf{P}^\top \cdot \mathbf{N} = 0 \quad \text{on } R = R_i \quad \text{and} \quad R = R_o, \tag{6}$$

where $\mathbf{N}$ is the unit outward normal in the reference configuration. Finally, Equations (6), (5), and (4) comprise the nonlinear elastic BVP [4].

To solve the BVP, Bevilacqua et al. leveraged radial symmetry to simplify the problem and find the baseline model. Specifically, using polar coordinates, they looked for a convenient, radially symmetric solution of the form

$$\varphi(X) = r(R)\,\mathbf{e}_r + Z\,\mathbf{e}_z. \tag{7}$$

Physically, this would mean that the twisting and bending of the cylindrical tube would not happen at the baseline. Next, I will briefly summarize their solution. First, from the incompressibility constraint (Equation (4)) the authors solved the differential equation and derive a relation between $r(R)$ and R:

$$r(R) = \sqrt{R^2 + r_i^2 - R_i^2}, \tag{8}$$

where r_i is the deformed inner radius of the heart tube. This provides the axisymmetric deformation mapping used as the base state for stability analysis. Using Newton's Second Law, the authors also found the Cauchy stress tensor (including radial, hoop, and shear stress) and Lagrange multiplier (hydrostatic pressure, p). Overall, the authors defined three dimensionless parameters which dictate the behavior of the system: $\tilde{\gamma} = \gamma R_o$: dimensionless torsion rate; $\alpha_R = R_o/R_i$: thickness ratio; $\alpha_L = L/R_o$: slenderness ratio [4].

After solving the symmetric BVP, the authors performed linear stability analysis of the finitely deformed tube using the theory of incremental deformations, the Stroh formulation, and the impedance matrix method. To assess when this axisymmetric solution becomes unstable, they considered the change in its configuration due to small perturbations. This mathematical analysis was complex and beyond the scope of this paper, but it included solving a system of ordinary differential equations and an Eigenvalue problem. In the end, the authors found the critical torsion rate at which instability (bending/looping) begins and how the geometry of the cylinder affects looping behavior [4]. To visualize and validate the

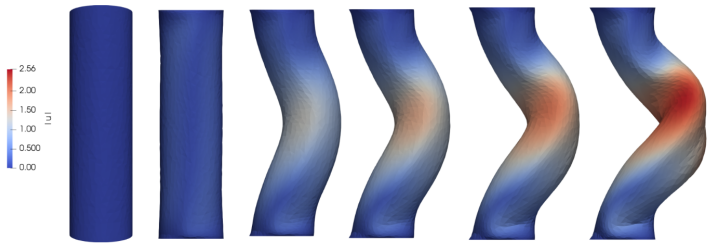

Figure 4: Configuration of the buckled tube when $\alpha_R = 2.85$, $\alpha_L = 7$, and Equation 9 holds. For this case, linear stability analysis gives $\tilde{\gamma} \approx 0.88$ [4].

post-buckling behavior around the critical point, the authors implemented a finite element simulation by meshing a 3D model of a hollow cylinder and imposing the boundary condition that there is zero displacement on the ends of the cylinder

(i.e., they are fixed):

$$\mathbf{u} = 0 \text{ on z=0, z= } \alpha_L. \tag{9}$$

Figure 4 shows the looping development of the modeled HT as the torsion parameter increases. Once the torsion parameter exceeds its linearly stable value, looping begins, stopping at the point at which the lumen closes in upon itself. These simulations reproduced the formation of a right-handed helical loop consistent with experimental observations of C-looping. By varying the thickness and slenderness ratios both within and outside the biologically relevant range, the model demonstrated how geometry influences the onset and morphology of looping. First, informed by experimental results, the authors varied the thickness and slenderness ratios, showing that as the torsion ratio increases, the cylinder twists into a helical pattern until the lumen closes in upon itself, representing the formation of the primitive 'valve'. The authors analyzed different cross-sectional shapes and performed a convergence analysis. Outside the normal biological range, the authors found that, for very thin tubes, looping occurred in a double helical mode, while, for very thick tubes, it occurred in a single loop mode, indicating the existence of threshold geometrical parameters which dictate looping patterns [4].

5 Comparative Evaluation of Models and Future Directions

The two models, Shi et al. (2014) and Bevilacqua et al. (2021), represent a classic dichotomy of experimental versus theoretical approaches to understanding developmental biomechanics. Both models provide novel approaches to the longstanding problem of embryonic cardiac looping, and each model has its strengths, limitations, and gaps. While Shi et al. focus on simulating active, force-driven morphogenesis on an anatomically exact HT structure, Bevilacqua et al. take a minimal, geometry-based approach in which looping emerges from a rigorous mathematical treatment of mechanical instability.

On one hand, Shi et al.'s integrated multiphysics model took into account decades of previous work, hypothesizing that, in embryonic C-looping, differential hypertrophic growth causes ventral bending while unbalanced loads exerted by the OVs on the HT determine looping directionality and a compressive load from the SPL causes torsion. As shown in Figure 3, their model incorporates a wide range of mechanical forces, including external compression from the SPL, asymmetric loading from the OVs, and intrinsic forces such as CJ swelling pressure and DM tension. Further, their mathematical model hinges on the assumptions that tissues are isotropic and pseudoelastic, and morphogenetic processes are applied anisotropically and are linearly time-dependent from stages 10-12. Major strengths of the Shi et al. (2014) model include the fact that it overcame all limitations with previous models – specifically, the fact that they are typically based on simplified geometry, and the fact that it integrates and handles multiple morphogenetic processes at once. This resulted in extremely strong agreement between experimental results and simulation from the frames of qualitative morphology, spatiotemporal trends, and perturbation results. Nonetheless, an incredibly realistic model such as this can come at the price of being convoluted, making it difficult to pinpoint which processes are causing the results. While the ability to accurately and robustly simulate cardiac looping is groundbreaking in and of itself, this paper did little to go beyond validation of their model, mainly sticking with perturbations that had been done experimentally in the past rather than leveraging the experimental power of the model with more combinations of perturbations. Further, the model was limited in not including OV fusion, mechanical feedback, and left-right asymmetry in DM growth as morphological processes. Increased experimentation with perturbation and padding the model with explicit modeling of those processes left out would be ideal next steps for the Shi et al. (2014) model. Further, the authors mentioned the need for more real-life experimental data, including noninvasive measurements of stress and strain fields, to make more progress on discovering biophysical mechanisms behind cardiac looping, but did not specify how this would occur. As imaging technology advances, elastography imaging of mechanical properties is one potential idea for making novel, noninvasive measurements of displacement fields in developing, looping hearts.

On the other hand, the Belivacqua et al. 2021 paper introduces a novel, theoretical, remodeling-induced buckling instability model used a rigorous mathematical treatment of mechanical instability of a hollow tube, along with a series of simulations, to demonstrate that geometric parameters identified in their theoretical model influence the onset and degree of twisting and bending in the modeled HT. Thus, Bevilacqua et al. provided significant support in favor of their hypothesis that torsional internal remodeling alone can drive the spontaneous onset and the fully nonlinear development of C-looping within its physiological range of geometrical parameters. The model elegantly captures key physical features of looping, neatly wrapping them into just three geometrical and material properties that dictate the torsional aspect of C-looping. Nonetheless, despite the mathematical complexity of this model, the simplicity of its physical model of the HT and the straightforwardness of its hypothesis most likely make it too good to be true. It is hard to believe that the theoretical model leveraging pure mathematics came several years after the experimental model leveraging technology.

Further developments would be needed to investigate if the symmetry break results from cell flow remodeling or external constraints and to put the mechanical instability model in the context of the true anatomy of the developing heart.

To this day, the biophysical mechanisms and functional significance of cardiac looping remain an open debate. Focusing on the torsional component of C-looping in the chick embryo, these two models manage to provide support for two different hypotheses: torsion is actively driven by external forces, including SPL compression and asymmetric loads from the OVs (Shi et al., 2014) and torsion arises spontaneously as a result of internal remodeling creating residual stress and geometrical frustration of the tube's structure, leading to buckling (Belivacqua et al., 2021). While Shi et al. do not rule out redundant minor forces leading to torsion, potentially including internal remodeling, it focuses on external morphogenetic processing acting on the HT, which is not modeled in Bevilacqua et al.'s paper. Due to Shi et al.'s superior anatomical modeling and more rigorous validation and review of literature, it seems more viable. So, how can the remodeling hypothesis be reconciled? The morphogenesis tensor chosen in Bevilacqua does not necessarily only represent internal remodeling; it could be a different, external process that produces similar forces and, thus, a similar looped configuration. In the future, the most promising models must integrate theoretical versus experimental models, find ways to study normal, in vivo stress and strain fields in developing embryos, and find a way to leverage the progress in genetic and molecular discovery in cardiac development to solve the mystery of the biomechanics of cardiac looping.

6 Integration With Developmental Principles

Throughout this course, we explored how mechanical forces and material properties shape morphogenesis, particularly in embryonic biological systems where large, nonlinear deformations demand more complex treatment than linear elasticity, which is often achieved numerically rather than analytically. Cardiac looping is a prime example of the intersection of mechanics and biology, which demonstrates that, even today, there remain unexplained, undiscovered mechanisms to tackle using technology, collaboration among different scientific fields, and discovery-based science. Both mathematical models discussed here are based on the theory of morphoelasticity. This framework assumes a stress-free intermediate configuration and uses growth (and other morphogenetic process) tensors to represent tissue remodeling. The mathematical models differ in their foundations – one is primarily empirical while the other is theoretical, which, similar to deciding the most appropriate mathematical framework (e.g., selecting Langrangian versus Eulerian frames or deciding which assumptions to make), is an important decision when approaching developmental biomechanics problems. Beyond mathematical modeling, other important decisions are displayed in the history of cardiac looping research, including consideration of evolutionary development to uncover functional reasons for nature's designs, selecting an appropriate model organism, and interpreting previous literature. While genetic and molecular cues are often conserved across species, the mechanical context of development – such as tissue material properties, anatomical constraints, and functional demands – can shape morphological outcomes. Sometimes, studying and taking into consideration different organisms, such as the detailed review [3] provides on fish cardiac looping, can offer new insights into functional significance by highlighting differences among organisms. Nonetheless, as a commodity, science directly related to human health is held paramount, which (along with experimental accessibility) is seen in the decision of many researchers to use chick embryos here. When interpreting the results in these cardiac looping experiments, it is critical to remember that multiple different processes or perturbations can lead to the same final configuration. This underscores the importance of distinguishing correlation from true causation. Einstein famously advised, "Make everything as simple as possible, but no simpler" – and, in the case of cardiac looping, the evidence suggests that oversimplified, single-mechanism explanations rarely capture the full picture. Instead, looping appears to emerge from the complex interplay of several biological demands and anatomical constraints.

7 Conclusion

Shi et al. (2014) and Bevilacqua et al. (2021) offer two valid but contrasting models for the biomechanics of torsion during cardiac looping based on external morphogenetic forces and internal stress and instability, respectively. Both reproduce experimental observations but differ in assumptions and scope. Future progress in describing the biophysical mechanisms of C-looping will require advanced mechanical property imaging, models that integrate genetic/molecular mechanisms with mechanical forces, and the consideration of the long list of forces present in the HT environment.

References

[1] Larry A. Taber. Biophysical mechanisms of cardiac looping. *International Journal of Developmental Biology*, 50(2-3):323–332, 2006.

[2] Yunfei Shi, Jiang Yao, Joshua M. Young, Jeffrey A. Fee, Riccardo Perucchio, and Larry A. Taber. Bending and twisting the embryonic heart: a computational model for c-looping based on realistic geometry. *Frontiers in Physiology*, 5:297, 2014.

[3] Jörg Männer. The functional significance of cardiac looping: Comparative embryology, anatomy, and physiology of the looped design of vertebrate hearts. *Journal of Cardiovascular Development and Disease*, 11(8):252, 2024.

[4] Giulia Bevilacqua, Pasquale Ciarletta, and Alfio Quarteroni. Morphomechanical model of the torsional c-looping in the embryonic heart. *SIAM Journal on Applied Mathematics*, 81(5):2103–2128, 2021.